Proceedings of Global Power and Propulsion Society
ISSN-Nr: 2504-4400
GPPS Hong Kong 2023
October 17-19, 2023
www.gpps.global

GPPS-TC-2023-0276

NONLINEAR FREQUENCY RESPONSE ANALYSIS OF A ROTATING STRUCTURE VIA THE HYPER-REDUCTION

Seung-Hoon Kang
Seoul National University
shkang94@snu.ac.kr
Seoul, Republic of Korea

Sangmin Lee
Seoul National University
sj7714@snu.ac.kr
Seoul, Republic of Korea

Minho Hwang
Seoul National University
hmh2989@snu.ac.kr
Seoul, Republic of Korea

Yongse Kim
Republic of Korea Air Force
upiop86@gmail.com
Daegu, Republic of Korea

Haeseong Cho
Jeonbuk National University
hcho@jbnu.ac.kr
Jeonju-si, Jeollabuk-do, Republic of Korea

SangJoon Shin
Seoul National University
ssjoon@snu.ac.kr
Seoul, Republic of Korea

ABSTRACT

Linear frequency response (LFR) analysis is the efficient approach to obtain the periodic vibratory response of the rotating structure, in which centrifugal effect is included by the preliminary nonlinear static analysis. However, LFR analysis is not capable of reflecting the coupling effect among the harmonic responses. Harmonic balance (HB) method overcomes such limitation by assuming the structural response as the truncated Fourier expansion. In this paper, HB analysis will be applied for the vibration prediction of the rotating structure. The difference from LFR analysis will be investigated. In addition, the hyper-reduction approach will be presented to treat the magnified degrees of freedom (DOFs) due to the harmonically coupled assumption. Proper orthogonal decomposition basis will be combined with the energy-conserving sampling and weighting method. Application on the example of 0.9-million DOFs will be conducted.

INTRODUCTION

A rotating structure suffers from various dynamic external loads which may bring a catastrophic vibratory response. Therefore, careful investigation on the vibration characteristics will be required during its design stage. Linear frequency response (LFR) analysis, in conjunction with the finite element (FE) method, is the conventional approach to obtain the periodic vibratory response. It assumes that the frequency of the structural response will be the same as that of the imposed external load (Ewins, 1998). For a rotating structure, effect of the centrifugal force should be considered especially for a high-aspect-ratio or slender configuration. The structure will be geometrically stiffened by the elongation. And at the same time, its stiffness will decrease, reflecting the increase of the centrifugal force equivalently. Such phenomena are referred as the stress-stiffening and spin-softening effects, respectively (Guo et al., 2001). Therefore, LFR analysis will be conducted through the pre-stressed and spin-softened stiffness which is obtained from the preliminary nonlinear static analysis.

Computational cost is another major concern for the numerical vibration analysis. The traditional mode superposition method, which employs the eigenmode as a reducing basis, might be the most powerful method to construct the reduced-order model (ROM) of the sole LFR analysis. However, the eigenmode will be inappropriate to be combined with the preliminary nonlinear static analysis. Under such background, Kang et al. (2022a,b) proposed an integrated ROM procedure from the nonlinear static to LFR analyses by using the proper orthogonal decomposition (POD) basis (Chatterjee, 2000). It was also revealed that conjunction with the hyper-reduction approach, e.g., energy-conserving sampling and weighting method (ECSW) (Farhat et al., 2014) employed in Kang et al. (2022a), was effective to additionally accelerate such ROM procedure.

Nevertheless, LFR analysis has a limitation to describe the coupling behavior among the harmonic responses, as well as with the non-harmonic one. The elongated structure due to the centrifugal force can be given as an example. For that, one-way procedure from the nonlinear static to LFR analyses will not be capable of predicting the amplification of the non-harmonic elongation by the harmonic load near the resonance. To overcome such limitation, the harmonic balance (HB) method (Krack and Gross, 2019) might be one of the most appropriate approaches. It assumes the structural response as the truncated Fourier expansions. As well as the non-harmonic components, it can predict the sub- or higher harmonic components according to the assumed harmonic order. Also, conjunction with the alternating frequency/time (AFT) scheme (Cameron and Griffin, 1989) facilitates the application of HB analysis on the nonlinear phenomena, e.g. geometrical, material and interfacial nonlinearities. Because the number of degrees of freedom (DOFs) extremely increases to couple the frequency components, ROM for HB analysis has also been actively investigated. Weeger et al. (2014) proposed a ROM framework of three-dimensional HB analysis using the eigenmode and its modal derivative as the reduced-basis. Morsy et al. (2023) presented the hyper-reduced HB analysis for the joint structure with a frictional behavior, using the augmented Jacobian projection method and ECSW. However, still few studies have attempted the HB method for the large-scale discretization, which is usually accompanied by the aero-mechanical analysis of a rotating component due to complicated configuration.

In this paper, HB method will be applied to the vibration prediction of a rotating structure. The difference from LFR analysis will be investigated. Then, the hyper-reduction approach for HB analysis will be proposed by using POD basis and ECSW. Application on the example of 0.9-million DOFs will be attempted.

PROBLEM STATEMENT

The dynamic equation of a rotating structure is written as Eq. 1.

$$\mathbf{M}\ddot{\mathbf{u}}(t)+\mathbf{f}^{\text{int}}(\mathbf{u}(t))=\mathbf{f}^{\text{ext}}(t)+\mathbf{f}_0^{\text{rot}}+\mathbf{K}^{\text{sp}}\mathbf{u}(t) \tag{1}$$

Herein, $\mathbf{M}\in\mathbb{R}^{N\times N}$ is a constant mass matrix, in which N is the number of DOFs generated by FE discretization. $\mathbf{u}\in\mathbb{R}^N$ and $\ddot{\mathbf{u}}\in\mathbb{R}^N$ is the displacement vector and its second-order time derivative. $\mathbf{f}^{\text{int}}\in\mathbb{R}^N$ and t is the internal force vector and time. The total external load is divided into the harmonic load $\mathbf{f}^{\text{ext}}\in\mathbb{R}^N$ and centrifugal force $\mathbf{f}_0^{\text{rot}}+\mathbf{K}^{\text{sp}}\mathbf{u}$, in which a constant rotating speed Ω is assumed. The centrifugal force is further divided into that of the initial configuration, $\mathbf{f}_0^{\text{rot}}\in\mathbb{R}^N$, and the increment $\mathbf{K}^{\text{sp}}\mathbf{u}$ due to the displacement. Here, $\mathbf{K}^{\text{sp}}\in\mathbb{R}^{N\times N}$ is the spin-softening matrix. For convenience, either configuration-dependant or non-harmonic external load is neglected except the centrifugal force. Damping effect, including Coriolis force, is also neglected. Rotating speed and related values, i.e., $\mathbf{f}_0^{\text{rot}}$ and $\mathbf{K}^{\text{sp}}$, are assumed to be constant.

In this section, governing equations and numerical procedure of LFR and HB analysis to solve Eq. 1 will be introduced briefly. And, their difference in the vibration prediction will be shown by a simple example.

Linear Frequency Response (LFR) Analysis

As aforementioned, LFR analysis assumes that the frequency of the structural response is the same as that of the harmonic external force, as written in Eq. 2.

$$\mathbf{f}^{\text{ext}}(t)=\mathbf{f}_c^{\text{ext}}\cos(\omega t)+\mathbf{f}_s^{\text{ext}}\sin(\omega t),\quad \mathbf{u}(t)=\mathbf{u}_c\cos(\omega t)+\mathbf{u}_s\sin(\omega t) \tag{2}$$

Here, $\mathbf{f}_c^{\text{ext}}\in\mathbb{R}^N$ and $\mathbf{f}_s^{\text{ext}}\in\mathbb{R}^N$ are the amplitude vectors of the harmonic external force, in which the subscript c and s denote the cosine and sine components. $\hat{\mathbf{u}}_c\in\mathbb{R}^N$ and $\hat{\mathbf{u}}_s\in\mathbb{R}^N$ are those of the displacement response. And, ω is the angular frequency of the harmonic external load.

Because the assumption of Eq. 2 is not capable of reflecting the non-harmonic centrifugal force, its contribution will be considered separately by the prerequisite nonlinear static analysis as written in Eq. 3.

$$\mathbf{f}^{\text{int}}(\bar{\mathbf{u}}_0)=\mathbf{f}_0^{\text{rot}}+\mathbf{K}^{\text{sp}}\bar{\mathbf{u}}_0 \tag{3}$$

Here, $\bar{\mathbf{u}}_0\in\mathbb{R}^N$ is the non-harmonic displacement vector by the centrifugal force. Through solving Eq. 3, $\bar{\mathbf{u}}_0$ and corresponding pre-stressed stiffness matrix $\bar{\mathbf{K}}^{\text{int}}=\mathbf{K}^{\text{int}}(\bar{\mathbf{u}}_0)\in\mathbb{R}^{N\times N}$ will be obtained. A detailed solution procedure is explained in Kang et al. (2022a).

Then, LFR analysis employs $\bar{\mathbf{K}}^{\text{int}}$, and assumes it to be constant. Eliminating the previously considered $\mathbf{f}_0^{\text{rot}}$ and assuming linear internal force, i.e., $\mathbf{f}^{\text{int}}(\mathbf{u}(t))=\bar{\mathbf{K}}^{\text{int}}\mathbf{u}(t)$, the governing equation of LFR analysis, Eq. 4, is derived by substituting Eq. 2 into Eq. 1.

$$\begin{bmatrix}\bar{\mathbf{K}}^{\text{int}}-\omega^2\mathbf{M}-\mathbf{K}^{\text{sp}} & \mathbf{0}_{N\times N}\\ \mathbf{0}_{N\times N} & \bar{\mathbf{K}}^{\text{int}}-\omega^2\mathbf{M}-\mathbf{K}^{\text{sp}}\end{bmatrix}\begin{Bmatrix}\mathbf{u}_c\\ \mathbf{u}_s\end{Bmatrix}=\begin{Bmatrix}\mathbf{f}_c^{\text{ext}}\\ \mathbf{f}_s^{\text{ext}}\end{Bmatrix} \tag{4}$$

Figure 1 shows the integrated procedure of LFR analysis for a rotating structure, which is simple due to the assumption of the identical frequency between the harmonic response and excitation (Eq. 2). However, it is not capable of predicting

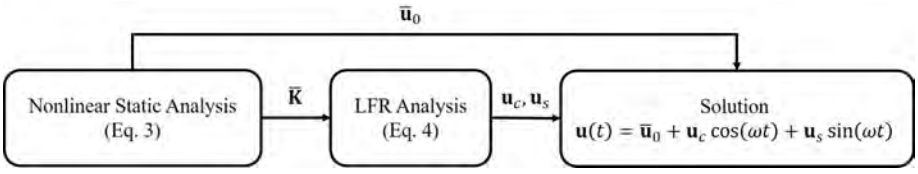

Figure 1 Numerical Procedure of a General LFR Analysis.

the coupling between the non-harmonic and harmonic response because the centrifugal and harmonic external load are considered in a separated manner. Also, the sub- or higher harmonic responses cannot be predicted.

Harmonic Balance (HB) Analysis

HB analysis assumes a structural response as the truncated Fourier expansion as written in Eq. 5.

$$\mathbf{f}^{\text{ext}}(t) = \sum_{k=1}^{m_f} \left(\mathbf{f}_{c,k}^{\text{ext}} \cos(k\omega t) + \mathbf{f}_{s,k}^{\text{ext}} \sin(k\omega t) \right), \quad \mathbf{u}(t) = \mathbf{u}_0 + \sum_{k=1}^{m_u} \left(\mathbf{u}_{c,k} \cos(k\omega t) + \mathbf{u}_{s,k} \sin(k\omega t) \right) \tag{5}$$

Here, $\mathbf{u}_0 \in \mathbb{R}^N$ is the non-harmonic displacement response. Expression for the non-harmonic external load $\mathbf{f}_0^{\text{ext}} \in \mathbb{R}^N$ is omitted, because the present study already considers $\mathbf{f}_0^{\text{ext}} = \mathbf{f}_0^{\text{rot}}$ in the dynamic equation (Eq. 1). An additional subscript k denotes the order of the harmonic components. m_f and m_u indicate the number of the harmonics of the external load and response, in which $m_f \leq m_u$.

To solve the dynamic equation (Eq. 1) combined with the coupled harmonic assumption (Eq. 5), the residual vector $\mathbf{r}_{\text{HB}} \in \mathbb{R}^{N_{HB}}$ and its linearized form is written as Eqs 6 and 7, respectively. $N_{HB} = (2m_u + 1)N$ is the number of DOFs of the HB analysis.

$$\mathbf{r}_{\text{HB}} = \mathbf{f}_{\text{HB}}^{\text{ext}} + \left(\mathbf{M}_{\text{HB}} + \mathbf{K}_{\text{HB}}^{\text{sp}} \right) \mathbf{u}_{\text{HB}} - \mathbf{f}_{\text{HB}}^{\text{int}} \tag{6}$$

$$\left(\left[\frac{\partial \mathbf{f}_{\text{HB}}^{\text{int}}}{\partial \mathbf{u}_{\text{HB}}} \right] - \left(\mathbf{M}_{\text{HB}} + \mathbf{K}_{\text{HB}}^{\text{sp}} \right) \right) \Delta \mathbf{u}_{\text{HB}} = \mathbf{r}_{\text{HB}} \tag{7}$$

$$\mathbf{f}_{\text{HB}}^{\text{ext}\,\top} = \left(2\mathbf{f}_0^{\text{rot}\,\top}, \mathbf{f}_{c,1}^{\text{ext}\,\top}, \mathbf{f}_{s,1}^{\text{ext}\,\top}, \cdots, \mathbf{f}_{c,m_f}^{\text{ext}\,\top}, \mathbf{f}_{c,m_f}^{\text{ext}\,\top}, \mathbf{0}_N^\top, \cdots, \mathbf{0}_N^\top \right) \tag{8}$$

$$\mathbf{f}_{\text{HB}}^{\text{int}\,\top} = \left(2\mathbf{f}_0^{\text{int}\,\top}, \mathbf{f}_{c,1}^{\text{int}\,\top}, \mathbf{f}_{s,1}^{\text{int}\,\top}, \cdots, \mathbf{f}_{c,m_u}^{\text{int}\,\top}, \mathbf{f}_{c,m_u}^{\text{int}\,\top} \right) \tag{9}$$

$$\mathbf{u}_{\text{HB}} = \left(\mathbf{u}_0^\top, \mathbf{u}_{c,1}^\top, \mathbf{u}_{s,1}^\top, \cdots, \mathbf{u}_{c,m_u}^\top, \mathbf{u}_{s,m_u}^\top \right) \tag{10}$$

$$\left(\mathbf{M}_{\text{HB}} + \mathbf{K}_{\text{HB}}^{\text{sp}} \right) = \begin{bmatrix} 2\mathbf{K}^{\text{sp}} & \mathbf{0}_{N\times N} & \mathbf{0}_{N\times N} & & \mathbf{0}_{N\times N} & \mathbf{0}_{N\times N} \\ \mathbf{0}_{N\times N} & \omega^2\mathbf{M} + \mathbf{K}^{\text{sp}} & \mathbf{0}_{N\times N} & \cdots & \mathbf{0}_{N\times N} & \mathbf{0}_{N\times N} \\ \mathbf{0}_{N\times N} & \mathbf{0}_{N\times N} & \omega^2\mathbf{M} + \mathbf{K}^{\text{sp}} & & \mathbf{0}_{N\times N} & \mathbf{0}_{N\times N} \\ & \vdots & & \ddots & & \vdots \\ \mathbf{0}_{N\times N} & \mathbf{0}_{N\times N} & \mathbf{0}_{N\times N} & & m_u^2\omega^2\mathbf{M} + \mathbf{K}^{\text{sp}} & \mathbf{0}_{N\times N} \\ \mathbf{0}_{N\times N} & \mathbf{0}_{N\times N} & \mathbf{0}_{N\times N} & \cdots & \mathbf{0}_{N\times N} & m_u^2\omega^2\mathbf{M} + \mathbf{K}^{\text{sp}} \end{bmatrix} \tag{11}$$

Here, $\Delta\mathbf{u}_{\text{HB}}$ indicates the increment of $\mathbf{u}_{\text{HB}}$.

To obtain the Fourier coefficient of the internal force $\mathbf{f}_{\text{HB}}^{\text{int}}$ and its gradient, AFT scheme (Cameron and Griffin, 1989) is conducted for each Newton-Raphson iteration. A detailed solution procedure is explained in Weeger et al. (2014) and Krack and Gross (2019). The different prediction between LFR and HB analysis will be shown by the simple example.

Numerical Example

The rotating beam of a high aspect ratio is shown in Fig. 2. The vibratory tip load, of which the angular frequency is indicated by ω, is imposed in its flapping and lead-lag direction. The length, width, and height of the beam are disretized by $9\times2\times1$ of 20-node hexahedral elements. To prevent the shear locking, reduced integration points are used for the calculation of the internal force and its displacement gradient. For the nonlinear static and HB analysis, the internal force and its gradient are obtained in the updated Lagrangian manner, in which the geometrical nonlinearity is considered. The modal characteristic is written in Table 1, which is obtained using the eigenvalue analysis. It explains that the rotation has

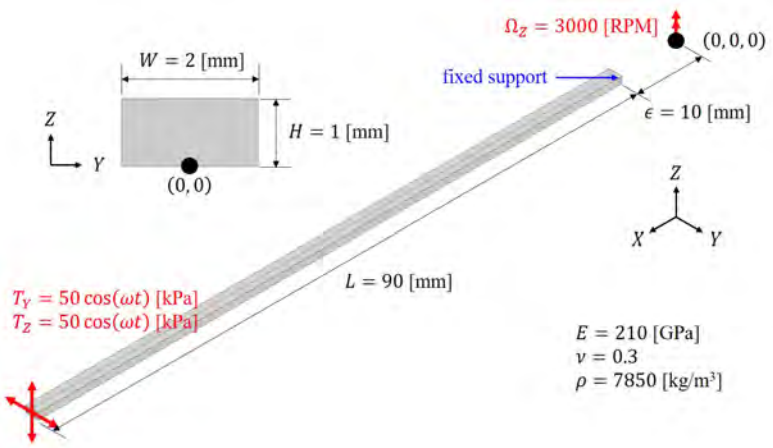

Figure 2 Beam Structure and the Analysis Condition.

Table 1 Modal Characteristics of the Beam.

Mode		Natural frequency	
Number	Characteristic	w/o Centrifugal effect	w/ Centrifugal effect
1	1st flapping mode	101.6 Hz	117.3 Hz
2	1st lead-lag mode	201.9 Hz	204.1 Hz

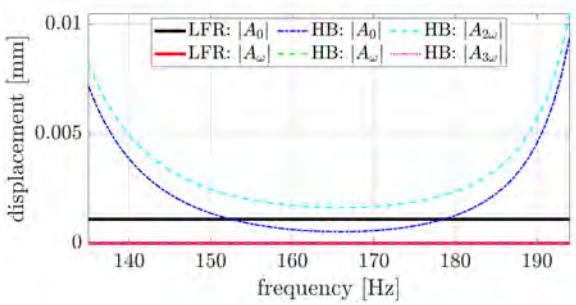

(a) Axial (X) Direction.

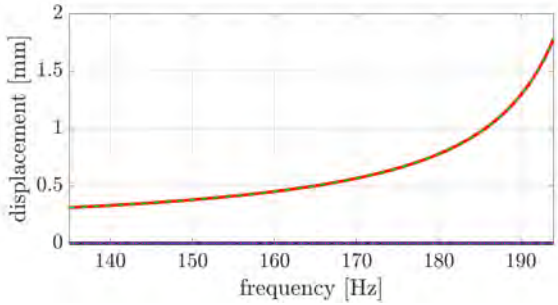

(b) Lead-lag (Y) Direction.

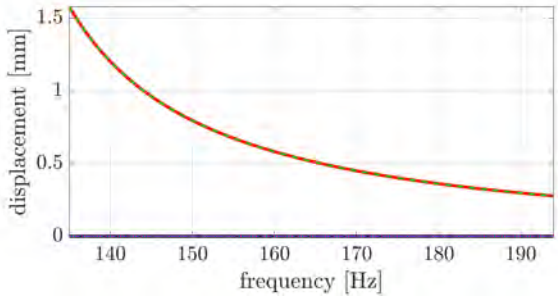

(c) Flapping (Z) Direction.

Figure 3 Displacement Amplitude at the Tip Center of the Beam in terms of the Imposed Frequency.

a significant effect on the dynamic characteristics and that the centrifugal effect should be considered before LFR analysis is initiated.

The analysis is conducted at the band between first two natural frequencies. The comparison between LFR and HB analysis is shown in Fig. 3. The results of LFR analysis includes that of the nonlinear static analysis to reflect the centrifugal effect. Because the deformation is infinitesimal, its components along with the harmonic excitation direction are almost identical between LFR and HB analysis. The difference occurs along with the axial direction, in which the non-harmonic centrifugal force acts. LFR analysis predicts the constant axial elongation in terms of the frequency of the external load. It is because of the one-way procedure to consider the centrifugal effect as previously shown in Fig. 1. In contrast, HB

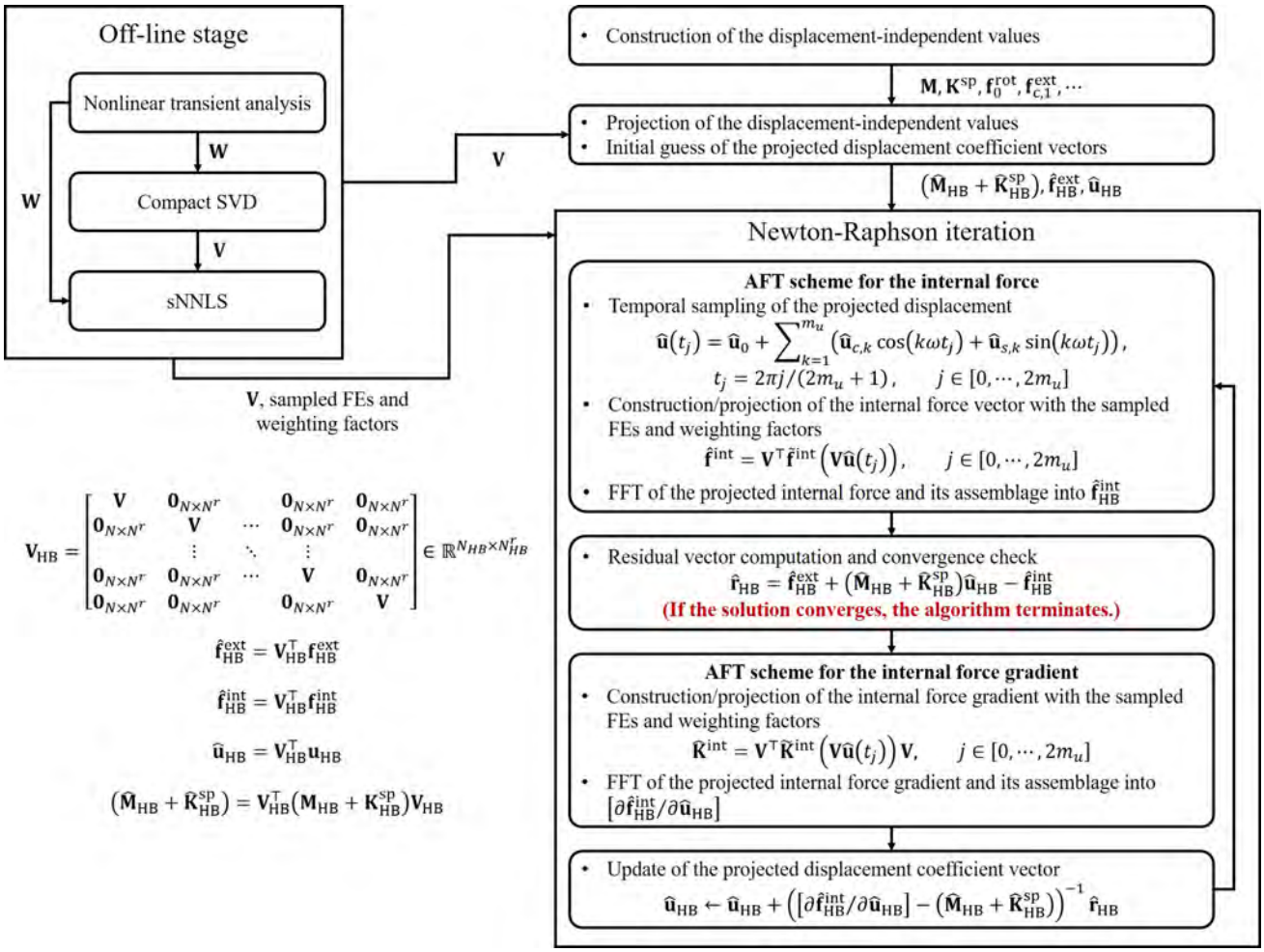

Figure 4 Present Numerical Framework of the Hyper-reduced HB Analysis.

analysis predicts the amplified axial elongation as the frequency of the harmonic load approaches the resonant regime. It is also noteworthy that the HB analysis captures the higher-harmonic axial vibration. Such behavior is related to the beam configuration, in which the transverse bending vibration in a single period induces the motion of the double period in the axial direction.

HARMONIC BALANCE (HB) ANALYSIS USING THE HYPER-REDUCTION

Nevertheless, the coupled assumption of HB analysis induces the increase of DOFs to be solved, which is proportional to the harmonic order m_u. Especially for the complicated configuration with large-scale discretization, unaffordable computational cost and memory requirement may occur. Repetitive computation of the internal force and its gradient included in AFT scheme is also non-negligible. To alleviate such cost, this section will present the hyper-reduced computational framework for HB analysis.

Figure 4 depicts the relevant framework. Current framework employs the projection-based ROM in which the POD mode (Chatterjee, 2000) is used as a reducing basis. ECSW method (Farhat et al., 2014) additionally alleviates the computational cost by approximating the projected internal force and its gradient as those constructed based on the sampled and weighted FEs. Computation is performed through MATLAB R2021a platform.

In the off-line stage, nonlinear time-transient analysis generates the training set, i.e., snapshot matrix $W \in \mathbb{R}^{N \times N_t}$. Here, N_t is the number of the training vectors. Detailed setup and the validation of the present transient analysis software can be found Kim et al. (2022). Then, POD basis is constructed by the compact singular value decomposition (SVD) of the snapshot matrix. And, lists of the sampled FEs and corresponding weighting factors are based on POD basis and time-transient training set, which are obtained by the sparse non-negative least square (sNNLS) algorithm (Lawson and Hanson, 1987; Farhat et al., 2014). It is noted that such list of the sampled FEs depends on the reduced bases and training set employed. sNNLS routine in the open-source YetAnotherFEcode (Jain et al., 2022) is employed.

Based on the above preparation, efficient HB analysis will be conducted. First, the values independent on the structural response, $\mathbf{M}$, $\mathbf{K}^{\mathrm{sp}}$, and $\mathbf{f}_0^{\mathrm{rot}}$, are projected upon the modal coordinates of the POD basis. For the harmonic external load $\mathbf{f}^{\mathrm{ext}}(t)$,

Figure 5 54H60 Propeller Blade and the Analysis Condition.

its Fourier coefficient vectors will be projected instead. Then, Newton-Raphson iteration will initiate. For each iteration, AFT scheme computes the temporal sampling of the projected internal vector $\hat{\mathbf{f}}^{\text{int}} = \mathbf{V}^{\top}\tilde{\mathbf{f}}^{\text{int}}$ and its gradient $\hat{\mathbf{K}}^{\text{int}} = \mathbf{V}^{\top}\tilde{\mathbf{K}}^{\text{int}}\mathbf{V}$. The upper tilde $\tilde{\square}$ indicates that the computations are performed only for the weighted and sampled FEs with the aid of ECSW method. $\mathbf{V} \in \mathbb{R}^{N\times N^r}$ is the projection matrix of which column vector is POD mode. Here, N^r is the number of POD modes employed. Then, Fourier coefficient of the projected internal force vector and its gradient are obtained through the fast Fourier transform (FFT). It is assembled to construct the reduced vector $\hat{\mathbf{f}}^{\text{int}}_{\text{HB}} \in \mathbb{R}^{N^r_{\text{HB}}}$ and the Jacobian matrix $\left[\partial\hat{\mathbf{f}}^{\text{int}}_{\text{HB}}/\partial\hat{\mathbf{u}}_{\text{HB}}\right] \in \mathbb{R}^{N^r_{\text{HB}}\times N^r_{\text{HB}}}$, in which $N^r_{\text{HB}} = (2m_u+1)N^r$. After the reduced increment $\Delta\hat{\mathbf{u}}_{\text{HB}} \in \mathbb{R}^{N^r_{\text{HB}}}$ is computed, Newton-Rapshon iteration continues until the convergence.

It is noted that the present framework be distinguished from that previously presented in Kang et al. (2022a). In the previous study, the one-way hyper-reduced ROM procedure from the nonlinear static analysis to LFR did not consider the coupling effect of the centrifugal elongation by the harmonic response. In addition, the interaction among the harmonic responses could not be predicted. In contrast, the present ROM framework is capable of considering the steady-state and harmonic responses simultaneously through the HB analysis.

RESULTS AND DISCUSSION

54H60 propeller blade, illustrated in Fig. 5, is chosen as a numerical example. Its slender configuration and high-aspect ratio induce the largely different prediction between the geometrically linear and nonlinear analysis as explained in Kim et al. (2022). Such configuration also contributes to the change of the vibratory behavior in terms of the rotational speed as introduced in Kang et al. (2022a). Application of 54H60 propeller blade to the parametric ROM framework considering a geometrically imperfection can be found in Kim et al. (2023). The harmonic load is imposed at the tip. The blade is discretized by 24,151 of 10-node tetrahedron FEs, of which the number of DOFs is $N = 133,587$. The number of the harmonics of the response is selected to be $m_u = 3$, requiring the DOFs of $N_{\text{HB}} = 935,109$ for the full-order model (FOM) HB analysis. It should be considered that the magnitude of the non-harmonic centrifugal force $\mathbf{f}^{\text{rot}}_0$ is usually larger than that of the harmonic load. Therefore, the non-harmonic and harmonic components of the residual vector, $\mathbf{r}_{\text{HB}}$ for FOM and $\hat{\mathbf{r}}_{\text{HB}}$ for ROM, are treated separately for the convergence check. Regarding to the computational resource, Intel i9-10900KF 3.70GHz CPU is employed.

Regarding the off-line stage, the imposed angular frequency ω of the transient analysis is set to be $\omega^{\text{off-line}} = 200\pi$ rad/s. Based on $\omega^{\text{off-line}}$, time-integration is conducted for 10 periods by 10 time steps per period ($N_t = 100$). The number of POD modes is selected to be $N^r = 50$, which extracts 218 FEs through sNNLS procedure. The sampled FEs are also shown in 5. Throughout the off-line stage, computational time of $T^{\text{off-line}} = 3,140$ s is spent.

To verify the robustness of the hyper-reduction approach, three cases of HB analysis is conducted for each FOM and ROM, while varying the imposed angular frequency ω. Analysis setup and the comparison are summarized in Table. 2. In that, the speed-up factor is estimated as $S = T^{\text{FOM}}/T^{\text{ROM}}$, in which the superscripts FOM and ROM denote the results obtain by the FOM and ROM analysis. It is shown that the present hyper-reduction procedure provides significant speed-up of HB analysis, approximately from 33 to 42 times faster than FOM analysis. The speed performance is still valid even when the off-line cost is considered. It can be shown by the effective speed-up factor $S_{\text{eff}} = \left(T^{\text{off-line}} + T^{\text{ROM}}_{\text{sum}}\right)/T^{\text{FOM}}_{\text{sum}}$, which is found to be 4.3. Here, the subscript sum indicates the total time spent for each FOM and ROM analysis. The relative discrepancy, calculated as $\|\mathbf{u}^{\text{FOM}}_{\text{HB}} - \mathbf{u}^{\text{ROM}}_{\text{HB}}\|_2/\|\mathbf{u}^{\text{FOM}}_{\text{HB}}\|_2$, shows that the present hyper-reduced framework is robust regardless of the imposed angular frequencies currently given. Figure 6 illustrates the displacement amplitude at the blade tip center for each harmonic response. The agreement between FOM and ROM analysis is found except for the order of $k = 3$ of which the magnitude is almost negligible.

However, the present hyper-reduction procedure has a limitation to be used in the general situation. Because the transient analysis is employed for the snapshot construction, it might be ambiguous to determine whether the training set

Table 2 Comparison between FOM and ROM for HB analysis.

Case	Imposed frequency	Computational time (FOM / ROM)	Speed-up	Relative Discrepancy
1	40 Hz	3,643 s / 107.7 s	33.8	0.29 %
2	100 Hz	7,216 s / 172.3 s	41.9	0.83 %
3	200 Hz	3,006 s / 81.69 s	36.8	0.21 %

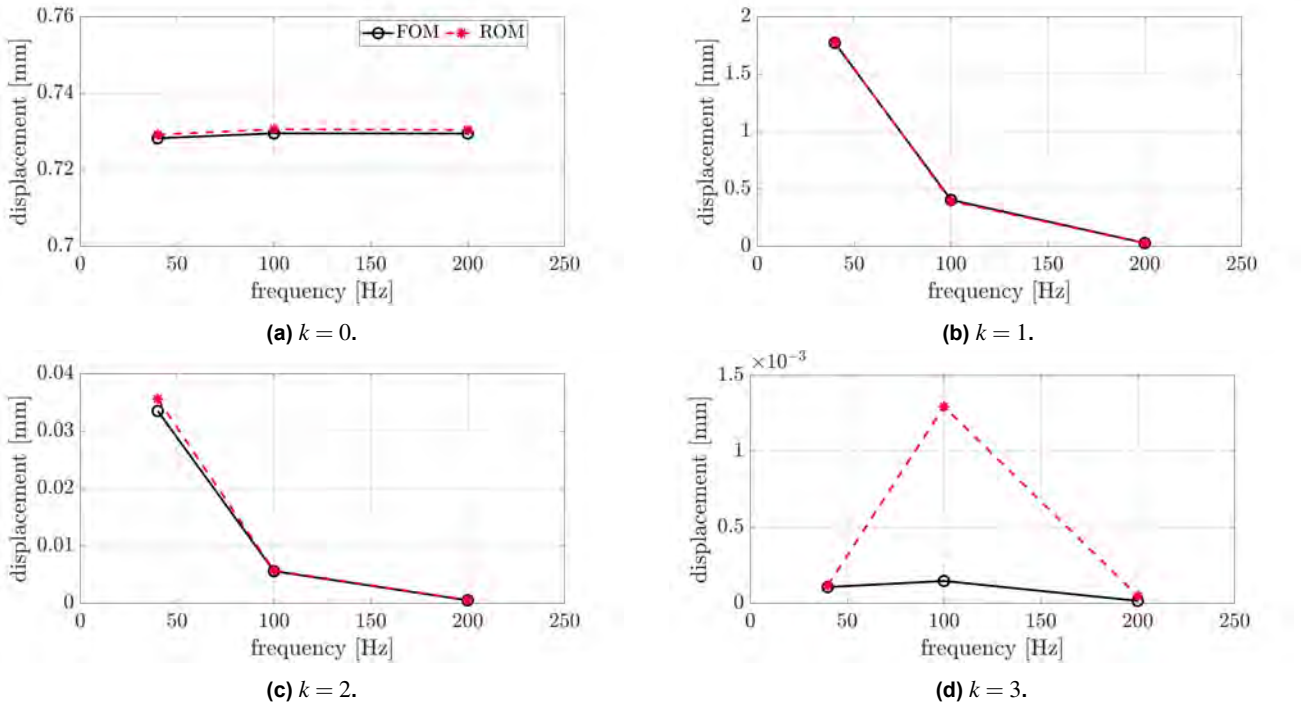

(a) $k = 0$. **(b)** $k = 1$.

(c) $k = 2$. **(d)** $k = 3$.

Figure 6 Displacement Amplitude at the Tip Center of the Propeller Blade in terms of the Imposed Frequency.

reaches the steady-state behavior. In addition, the transient analysis will spend tremendous time steps to reach the steady-state for the component of higher stiffness-to-mass ratio with less damping. Thus, the future work will be concentrated on the development of an efficient and standardized training set generation appropriate to the HB analysis.

CONCLUSIONS

In this paper, application of HB analysis on a rotating structure is investigated to overcome the limitation of the conventional LFR anlaysis. By the example of a simple beam structure, capability of HB analysis to predict the coupling among non-harmonic response and harmonic responses is demonstrated well. To deal with the increased number of DOFs to treat the coupling behavior, this paper also presents the hyper-reduced approach for HB analysis. It is based on the POD mode and ECSW method, of which the snapshot matrix is collected through the nonlinear time transient analysis. Application on the propeller blade of 0.9-million DOFs is presented. It is found that current hyper-reduction approach is faster than FOM, about 33 to 42 times in terms of the speed-up. Considering the off-line stage, effective speed-up of 4.3 is found for the simulation of three cases. Also, the accuracy of ROM is validated in terms of the relative displacement discrepancy.

Nevertheless, the present hyper-reduced HB analysis depends on the off-line stage by the time-transient analysis, which can be ambiguous to treat for the general cases. Therefore, the model-driven approach is being investigated to establish a standardized hyper-reduction framework for the HB analysis of a rotating structure.

ACKNOWLEDGMENTS

This work was supported by the Agency For Defense Development Grant funded by the Korean Government (UD220004JD).

References

Cameron, T. M. and Griffin, J. H. (1989), 'An alternating frequency/time domain method for calculating the steady-state response of nonlinear dynamic systems', *J. Appl. Mech.* **56**(1), 149–154.
URL: *https://doi.org/10.1115/1.3176036*

Chatterjee, A. (2000), 'An introduction to the proper orthogonal decomposition', *Curr. Sci.* **78**(7), 808–817.
URL: *https://www.jstor.org/stable/24103957*

Ewins, D. J. (1998), Basic structural dynamics, *in* M. F. Platzer and F. O. Carta, eds, 'AGARD Manual on Aeroelasticity in Axial-Flow Turbomachines - Volume 2: Structural Dynamics and Aeroelasticity', North Atlantic Treaty Organization (NATO), Neuilly sur Seine, pp. 31–46.

Farhat, C., Avery, P., Chapman, T. and Cortial, J. (2014), 'Dimensional reduction of nonlinear finite element dynamic models with finite rotations and energy-based mesh sampling and weighting for computational efficiency', *Int. J. Numer. Methods Eng.* **98**(9), 652–662.
URL: *https://doi.org/10.1002/nme.4668*

Guo, D., Chu, F. L. and Zheng, Z. C. (2001), 'The influence of rotation on vibration of a thick cylindrical shell', *J. Sound Vib.* **242**(3), 487–505.
URL: *https://doi.org/10.1006/jsvi.2000.3356*

Jain, S., Marconi, J. and Tiso, P. (2022), 'YetAnotherFEcode; release v1.3.0'.
URL: *http://doi.org/10.5281/zenodo.4011281*

Kang, S. H., Kim, Y., Cho, H. and Shin, S. J. (2022a), 'Improved hyper-reduction approach for the forced vibration analysis of rotating components', *Comput. Mech.* **69**, 1443–1456.
URL: *https://doi.org/10.1007/s00466-022-02149-y*

Kang, S. H., Kim, Y., Song, D., Cho, H. and Shin, S. J. (2022b), 'Numerical characterization of turbine blade dynamic properties via proper orthogonal decomposition', *J. Phys. Conf. Ser.* **2217**, 012034.
URL: *https://doi.org/10.1088/1742-6596/2217/1/012034*

Kim, Y., Kang, S. H., Cho, H., H., K. and Shin, S. J. (2023), 'Parametric reduced-order modeling enhancement for a geometrically imperfect component via hyper-reduction', *Comput. Methods Appl. Mech. Eng.* **403**, 115701.
URL: *https://doi.org/10.1016/j.cma.2022.115701*

Kim, Y., Kang, S. H., Cho, H. and Shin, S. J. (2022), 'Improved nonlinear analysis of a propeller blade based on hyper-reduction', *AIAA J.* **60**(3), 1909–1922.
URL: *https://doi.org/10.2514/1.J060742*

Krack, M. and Gross, J. (2019), *Harmonic Balance for Nonlinear Vibration Problems*, Springer, Cham.
URL: *https://doi.org/10.1007/978-3-030-14023-6*

Lawson, C. L. and Hanson, R. J. (1987), *Solving Least Squares Problems*, Society for Industrial and Applied Mathematics (SIAM), Philadelphia.

Morsy, A. A., Kast, M. and Tiso, P. (2023), 'A frequency-domain reduced order model for joints by hyper-reduction and model-driven sampling', *Mech. Syst. Signal Process* **185**, 109744.
URL: *https://doi.org/10.1016/j.ymssp.2022.109744*

Weeger, O., Wever, U. and Simeon, B. (2014), 'Nonlinear frequency response analysis of structural vibrations', *Comput. Mech.* **54**, 1477–1495.
URL: *https://doi.org/10.1007/s00466-014-1070-9*